Forward and inverse cascades by exact resonances in surface gravity waves

Zhou Zhang and Yulin Pan [*]

Department of Naval Architecture and Marine Engineering, University of Michigan, Ann Arbor, Michigan 48109, USA

We study the energy transfer by exact resonances for deep-water surface gravity waves in a finite periodic spatial domain. Based on a kinematic model simulating the generation of active wave modes in a finite discrete wave number space $\mathcal{S}_R$, we examine the possibility of direct and inverse cascades. More specifically, we set an initially excited region which iteratively spreads energy to wave modes in $\mathcal{S}_R$ through exact resonances. At each iteration, we first activate new modes from scale resonances (which generate modes with new lengths), then consider two bounding situations for angle resonances (which transfer energy at the same length scale): the lower bound where no angle resonance is included and the upper bound where all modes with the same length as any active mode are excited. Such a strategy is essential to enable the computation for a large domain $\mathcal{S}_R$ with the maximum wave number $R \sim 10^3$. We show that for both direct and inverse cascades, the modal propagation to the boundaries of $\mathcal{S}_R$ can be established when the initially excited region is sufficiently large; otherwise a frozen turbulence state occurs, with a sharp transition between the two regimes especially for the direct cascade. Through a study on the structure of resonant quartets, the mechanism associated with the sharp transition and the role of angular energy transfer in the cascades are elucidated.

I. INTRODUCTION

Wave turbulence theory (WTT) describes the statistical behavior of a large number of dispersive waves subject to nonlinear interactions [1]. In the framework of WTT, the wave system is described by a kinetic equation (KE) which has stationary solutions of the Kolmogorov-Zakharov power-law spectra in the inertial range. Analogous to the Kolmogorov description of hydrodynamic turbulence, WTT predicts energy cascades through scales with a constant energy flux in the inertial range. This methodology has been applied to a wide variety of physical systems including surface gravity waves [2], capillary waves [3], internal gravity waves [4], plasma waves [5], and gravitational waves [6].

In spite of its fruitful applications, WTT is based on the assumption of an infinite spatial domain, which is usually not achieved in both numerical and laboratory experiments. For a finite system, the wave number space becomes discrete with the spacing between adjacent wave modes $\Delta k = 2\pi/L$, where L is the size of the domain. Under this situation, it has been understood that the predictions from KE can be obtained only if the nonlinearity level is sufficiently high. The dynamics in this regime is governed by the so-called kinetic wave turbulence, where quasiresonances play a dominant role in energy transfer, as shown in numerical simulations [7–11] and pure analysis [12,13]. When the nonlinearity level is sufficiently low for a fixed domain size (or the domain size is sufficiently small for a given nonlinearity level), the discreteness in the wave number space becomes dominant over nonlinear broadening and the quasiresonances are prohibited. Such situations

may occur in both experiments and simulations, as discussed in [14,15] for a wave tank of realistic size. Physically, this dynamical regime is called the discrete wave turbulence regime (see simulation evidence in [8,16] and pure analysis in [17]), where the cascade can be excited only through exact resonances, i.e., modal interactions satisfying

$$\boldsymbol{k}_1 \pm \boldsymbol{k}_2 \pm \cdots \pm \boldsymbol{k}_s = 0,$$
$$\omega_1 \pm \omega_2 \pm \cdots \pm \omega_s = 0, \tag{1}$$

where $\boldsymbol{k}_i = (m_i, n_i)$ (after canceling the common factor Δk assuming a square spatial domain for simplicity) is the discrete wave number vector with $m_i, n_i \in \mathbb{Z}$ and ω_i is the angular frequency determined from the dispersion relation, say, $\omega_i \sim k_i^\alpha$ with $k_i = |\boldsymbol{k}_i|$. The importance of (1) in understanding the wave dynamics at low nonlinearity has been demonstrated in capillary wave turbulence [18–20], MMT turbulence [16], and surface gravity wave turbulence [21–23] (also see review in [24]).

The study on the exact resonances in discrete wave number space is a main subject of discrete wave turbulence (DWT), introduced first by Kartashova [25–27]. In general, the problem of computing exact resonances in a discrete wave number space is to find integer solutions of (1), which is essentially a system of Diophantine equations. The properties of solutions in different wave systems are determined by the values of s in (1) and α in the dispersion relation. In particular, there are certain wave systems in which no exact resonance exists (e.g., capillary waves with $s = 3$, $\alpha = 3/2$) [27], as well as systems containing a large number of exact resonances so that the energy can be transferred to arbitrarily large wave numbers [e.g., the nonlinear Schrödinger (NLS) equation with $s = 4$, $\alpha = 2$] [28,29].

[*]yulinpan@umich.edu

The situation for deep-water surface gravity waves ($s = 4$, $\alpha = 1/2$) is much more complicated. Previous studies have shown that exact resonances exist, but are sparse other than some trivial quartet solutions (which do not excite new modes in scale) [15,30,31]. However, it is not clear what should be expected from these exact resonances in a discrete wave number domain $\mathcal{S}_R$ (given some initially active modes), i.e., whether a state of unlimited cascade or frozen turbulence is relevant. More precisely, here we define the propagation of wave modes generated by exact resonances from the initial region to the maximum wave number R in $\mathcal{S}_R$ as an "unlimited cascade (in $\mathcal{S}_R$)" and otherwise as "frozen turbulence". We note that the concept of "frozen turbulence" was originally provided in [18] for capillary waves, which indicates a state where no new modes can be generated by exact resonances so that the turbulent cascade has to be "frozen". Here we use a generalized definition to describe the bounded genera-tion of wave modes by exact resonances. For $R \rightarrow \infty$, this is a very hard number theoretical problem (through private communication with number theorists), which is beyond our scope in this paper. We will instead consider an $\mathcal{S}_R$ with finite $R \sim 10^3$ (the maximum R in this study is 2500), which is compatible with (or beyond) most state-of-the-art simulations [8,23,30,32–37] performed for wave turbulence (with the only exception of [38] to the authors' knowledge).

An effective approach to study the above problem numeri-cally is the so-called kinematic method, i.e., with an initial set of active modes, the generation of new modes to outer regions is computed iteratively by finding solutions to (1). Under the kinematic method, we consider the modal propagation toward higher and lower wave numbers direct and inverse cascades respectively. This method has been applied to capillary waves [39], gravity waves [30], and NLS [40], which, however, mainly focus on the effect of exact or quasiresonances in a small domain, i.e., with small R. As an example, for gravity waves, the only available result is for $R = 64$ with initially active modes in $k \in [6, 9]$ (i.e., wave number magnitude in the interval from 6 to 9), where it is shown in [30] that a frozen turbulence state is observed. The difficulty in extending the existing kinematic method to our interest of $R \sim 10^3$ lies in the computational cost. A brute-force search of solution of (1), as applied in [30], exhibits a computational cost that grows fast with the increase of the number of active modes (in particular the cost scales as the cubic of active mode numbers for each iteration). Therefore, in order to make cases of $R \sim 10^3$ computationally tractable, a much more efficient numerical method needs to be developed for the kinematic study.

One way to save some computational cost is to precompute the set Q of all exact resonances within $\mathcal{S}_R$ using a fast generic method [31,41,42]. With the invariant set Q available, we can loop over Q to compute the energy spreading in each iteration, instead of a much larger set of all combinations of the activated modes (that expands up to $O(10^{18})$ if all modes in $\mathcal{S}_R$ are excited when $R = 1000$). However, this is still not sufficient due to the large number of elements in Q, with $|Q| \sim 10^8$. In order to further reduce the computational cost, we consider a small subset Q_s of Q (with $|Q_s| \sim 10^4$) that includes only the scale resonances, i.e., resonances generating wave modes with new length that are of vital importance to

the cascade. The remaining set Q_a (with $|Q_a| \sim 10^8$) contains only angle resonances with pairwise equal lengths ($|\boldsymbol{k}_1| = |\boldsymbol{k}_3|$ and $|\boldsymbol{k}_2| = |\boldsymbol{k}_4|$; or $|\boldsymbol{k}_1| = |\boldsymbol{k}_4|$ and $|\boldsymbol{k}_2| = |\boldsymbol{k}_3|$) that are less important (but may play a role in connecting different scale resonances). Accordingly, we can formulate an efficient computational scheme to loop over Q_s in each iteration and account for the resonances in Q_a by its two bounds: an lower bound that no angle resonances are included and an upper bound that all modes with equal length with any active one are excited. Using this scheme, the computational cost for $R \sim 10^3$ becomes affordable, and we are certain that the true solution lies between the two bounds of the computation, which is sufficient for the physical purpose in this study.

In this paper, we apply the computational method outlined above to study the resonant energy transfer of surface gravity waves in a finite discrete wave number space with $R = 2500$. The initially active modes are placed in a circular region with radius r_D for the direct cascade. We show that for small r_D, a state of frozen turbulence is observed with the maximum reachable wave number $k_{\max}$ linearly proportional to r_D. At $r_D \sim [60, 110]$, a sharp transition to unlimited cascade oc-curs where $k_{\max} \sim R$ is established for both upper and lower bounds. In addition to the direct cascade, we also study the inverse cascade with initial active modes in a ring-shaped area, and we show the transition from frozen turbulence to unlimited cascade (under their corresponding definitions in the context of inverse cascade) with the increase of the thick-ness of the ring. Finally, we analyze the structure of resonant quartets, through which the sharp transition from frozen turbu-lence to unlimited cascade is explained, and the role of angle resonances in determining the extent of the modal propagation is elucidated for both direct and inverse cascades.

II. METHODOLOGY

We consider the surface gravity wave system with resonant conditions in the form

$$\boldsymbol{k}_1 + \boldsymbol{k}_2 = \boldsymbol{k}_3 + \boldsymbol{k}_4,$$
$$\sqrt{k_1} + \sqrt{k_2} = \sqrt{k_3} + \sqrt{k_4}, \tag{2}$$

where $\boldsymbol{k}_i = (m_i, n_i)$ and $k_i = |\boldsymbol{k}_i|$ ($i = 1, 2, 3, 4$) with $m_i, n_i \in \mathbb{Z}$ and $\sqrt{m_i^2 + n_i^2} \leqslant R$ for a given $R \in \mathbb{N}$. The solutions of (2) correspond to the exact resonances in a finite wave number domain $\mathcal{S}_R = \{\boldsymbol{k} \in \mathbb{Z}^2 : k \leqslant R\}$. In our kinematic model, we specify the initial condition by defining a set of active modes denoted by $\mathcal{S}_0$. For the direct cascade, the initially active modes are placed in a circular area $\mathcal{S}_0 = \{\boldsymbol{k} \in \mathbb{Z}^2 : k \leqslant r_D\}$ where $0 < r_D < R$. For the inverse cascade, they are placed in a ring-shaped area $\mathcal{S}_0 = \{\boldsymbol{k} \in \mathbb{Z}^2 : r_I \leqslant k \leqslant R\}$ where $0 < r_I < R$.

The solution for the direct or inverse cascade problem now amounts to iteratively finding the solution of (2) for energy spreading; i.e., for each iteration, we loop over all combina-tions of three active modes and check whether there exists a fourth mode satisfying (2). Such a brute-force method, as reviewed, is not computationally affordable for large $R \sim 10^3$. Here we propose an efficient method for this computation providing the upper and lower bounds of the true solution that are sufficient for our physical purpose. The first step is to

precompute (before the start of the iterations) the set of scale resonances $\mathcal{Q}_s$ inside the spectral domain $\mathcal{S}_R$:

$$\mathcal{Q}_s = \{(\boldsymbol{k}_1, \boldsymbol{k}_2, \boldsymbol{k}_3, \boldsymbol{k}_4) : \boldsymbol{k}_1 + \boldsymbol{k}_2 = \boldsymbol{k}_3 + \boldsymbol{k}_4,$$
$$\sqrt{k_1} + \sqrt{k_2} = \sqrt{k_3} + \sqrt{k_4},$$
$$k_1 \neq k_3, \; k_1 \neq k_4,$$
$$\boldsymbol{k}_i \in \mathcal{S}_R, \; \forall \, i = 1, 2, 3, 4\}. \tag{3}$$

As shown by Kartashova, the scale resonances in $\mathcal{Q}_s$ are substantially sparser compared to all resonances (or angle resonances) [43,44] and can be computed by a fast algorithm [31]. The principle of this algorithm is that only a small subset of numbers need to be considered for frequency ω according to the irrationality of the dispersion relation, which substantially reduces the number of searches (since only the small subset and the corresponding wave numbers need to be searched instead of all wave numbers). We present the detailed algorithm to compute $\mathcal{Q}_s$ in the Appendix mainly following [31]. The overall computational complexity can be estimated as $O(R^2)$, which needs to be performed only once for all kinematic calculations in this paper.

With $\mathcal{Q}_s$ available, we can iteratively update the set of active modes $\mathcal{S}_i$ ($i = 1, 2, \ldots, N$) starting from $\mathcal{S}_0$ with operation $\mathcal{S}_{i+1} = \boldsymbol{P}^s(\mathcal{S}_i)$. In particular, in performing $\boldsymbol{P}^s$, we loop over all the quartets in $\mathcal{Q}_s$, and if there exist three (and only three) active modes (according to $\mathcal{S}_i$) in one quartet, we activate the fourth one. The set $\mathcal{S}_{i+1}$ is then taken as the union of $\mathcal{S}_i$ and all newly activated modes. Since $\mathcal{Q}_s$ is invariant and sparse, the number of calculations at each iteration is a small constant, as opposed to the situation in the brute-force approach.

To further account for the effects of angle resonances, two bounds of the result can be considered. The lower bound can be simply taken as $\mathcal{S}_i^l = \mathcal{S}_i$ ($i = 1, 2, \ldots, N^l$), i.e., result of spreading only from scale resonances. For the upper bound, we consider the situation that at each iteration, after the spreading by scale resonances, we activate all modes in S_R that have the same length with any active modes (defined as operation $\boldsymbol{P}^a$). More precisely, we perform $\mathcal{S}_{i+1}^u = \boldsymbol{P}^s(\mathcal{S}_i^u) \cup \boldsymbol{P}^a[\boldsymbol{P}^s(\mathcal{S}_i^u)]$ ($i = 1, 2, \ldots, N^u$) from $\mathcal{S}_0^u = \mathcal{S}_0$, where the operation $\boldsymbol{P}^a$ is defined as $\boldsymbol{P}^a[\mathcal{S}^*] = \{\boldsymbol{k} : k = k_1, \forall \boldsymbol{k}_1 \in \mathcal{S}^*\}$. The full algorithm for the computation is presented in Algorithm 1, with the code available on Github [45].

III. RESULTS

We first present results for direct cascade in a wave number domain of $R = 2500$ using our kinematic model. Figure 1 shows the upper and lower bounds of final distributions of active modes (i.e., no more activated modes in the next iteration) for three cases with $r_D = 50, 80, 120$. For $r_D = 50$ as in Figs. 1(a) and 1(b), the results from the upper and lower bounds are identical, indicating a true solution of frozen turbulence with maximum reachable wave number $k_{\max} = 243$. For $r_D = 80$ as in Figs. 1(c) and 1(d), a difference in the upper and lower bounds of the solution is observed, showing that the true solution $k_{\max}$ lies in a relatively large range of [729,2401], still a state of frozen turbulence according to our definition. Finally, for $r_D = 120$ as in Figs. 1(e) and 1(f), the upper and lower bounds become much closer, both close to

Algorithm 1. Kinematic model.

Input: size of domain R, the radius r_D for direct cascades or the inner radius r_I for inverse cascades
Output: the final sets of active modes $\mathcal{S}_{N^l}^l$ for lower bound and $\mathcal{S}_{N^u}^u$ for upper bound

    Initialization initialize the set of active modes $\mathcal{S}_0 = \{\boldsymbol{k} \in \mathbb{Z}^2 : k \leqslant r_D\}$ for direct cascades or $\mathcal{S}_0 = \{\boldsymbol{k} \in \mathbb{Z}^2 : r_I \leqslant k \leqslant R\}$ for inverse cascades

    Calculate $\mathcal{Q}_s$ from (2)
    $i \leftarrow 0, \mathcal{S}_0^l \leftarrow \mathcal{S}_0$
    while $\mathcal{S}_i^l \neq \boldsymbol{P}^s(\mathcal{S}_i^l)$ **do**
        $\mathcal{S}_{i+1}^l \leftarrow \boldsymbol{P}^s(\mathcal{S}_i^l)$
        $i \leftarrow i + 1$
    end while
    $N^l \leftarrow i$
    $i \leftarrow 0, \mathcal{S}_0^u \leftarrow \mathcal{S}_0$
    while $\mathcal{S}_i^u \neq \boldsymbol{P}^s(\mathcal{S}_i^u)$ **do**
        $\mathcal{S}_{i+1}^u \leftarrow \boldsymbol{P}^s(\mathcal{S}_i^u) \cup \boldsymbol{P}^a[\boldsymbol{P}^s(\mathcal{S}_i^u)]$
        $i \leftarrow i + 1$
    end while
    $N^u \leftarrow i$
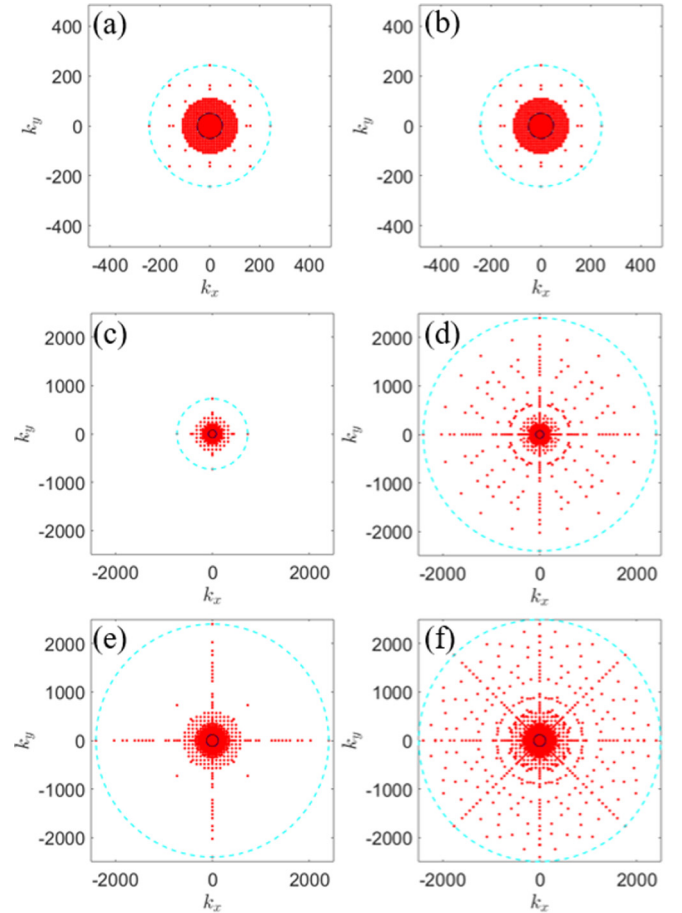
FIG. 1. The distribution of active wave modes (red dots) in the final state of direct cascades in a domain with $R = 2500$, for (a) $r_D = 50$, lower bound, (b) $r_D = 50$, upper bound, (c) $r_D = 80$, lower bound, (d) $r_D = 80$, upper bound, (e) $r_D = 120$, lower bound, and (f) $r_D = 120$, upper bound. The initially excited region is indicated by a red area circled by a black solid line. The maximum wave number $k_{\max}$ of the active modes is indicated by a circle with cyan dashed line.
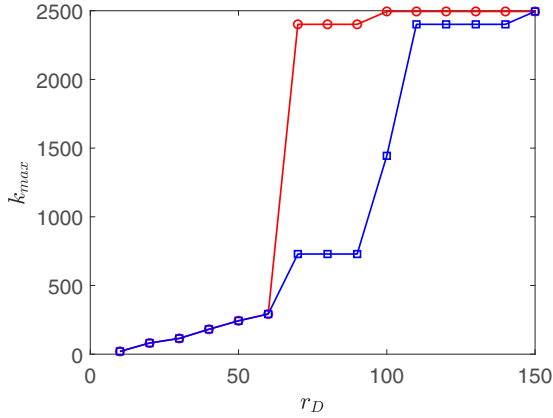
FIG. 2. The maximum wave number k_{max} as a function of the radius of the initial region r_D in direct cascades with $R = 2500$. Both upper (red line with squares) and lower (blue line with squares) bounds are shown.

the outer boundary of the domain with $k_{max} \sim R$, indicating a state of unlimited cascade. This is in spite of the fact that the upper-bound solution is associated with a much denser active modes excited by angle resonances.

A more complete view of the relation between k_{max} and r_D is shown in Fig. 2 with both upper and lower bounds of the solution. We see that there exists a sharp transition between frozen turbulence and unlimited cascade for a critical value of $r_D \sim [60, 110]$ (considering the uncertainty exhibited between upper and lower bounds). For r_D below the critical value, a frozen turbulence state is observed with exact match of upper and lower bounds of the solution, showing a linear relation fitted by $k_{max} \approx 5.5 r_D - 35.9$. For r_D above the critical value, the state quickly transits to unlimited cascade with $k_{max} \gg r_D$ (and eventually $k_{max} \sim R$). Such a transition implies a bifurcation of solutions depending on the initial condition of energy distribution in discrete turbulence of surface gravity waves. In addition, we remark that the frozen turbulence observed here for small r_D is consistent with the simulation of primitive Euler equations at low nonlinearity level [23], which suggests a frozen turbulence state when the forcing is located in the range of $k \in [1, 19]$.

We next present the results for inverse cascade with initial active modes placed in a ring with radius $[r_I, R]$. Our interest is to understand the effect of ring thickness on the minimum wave number k_{min} reachable in the cascade. For this purpose, we keep $r_I = 1000$ as a constant and vary R to examine its effect on the inverse cascades. Figure 3 shows the upper and lower bounds of final distributions of active modes in inverse cascades for $R = 1400$, 1700, and 2200. For $R = 1400$ as in Figs. 3(a) and 3(b), a frozen turbulence state is observed with no new active modes generated (for both upper and lower bounds). For $R = 1700$ as in Figs. 3(c) and 3(d), k_{min} reaches [492.4, 176.7] according to the two bounds of solution, indicating again a state of frozen turbulence. The unlimited cascade is enabled as in Figs. 3(e) and 3(f) for $R = 2200$, where $k_{min} \sim 1$ (the fundamental mode) from both the upper and lower bounds.

We show a more complete view of the relation between k_{min} and R in Fig. 4. For $R \leqslant 1500$, no new modes can
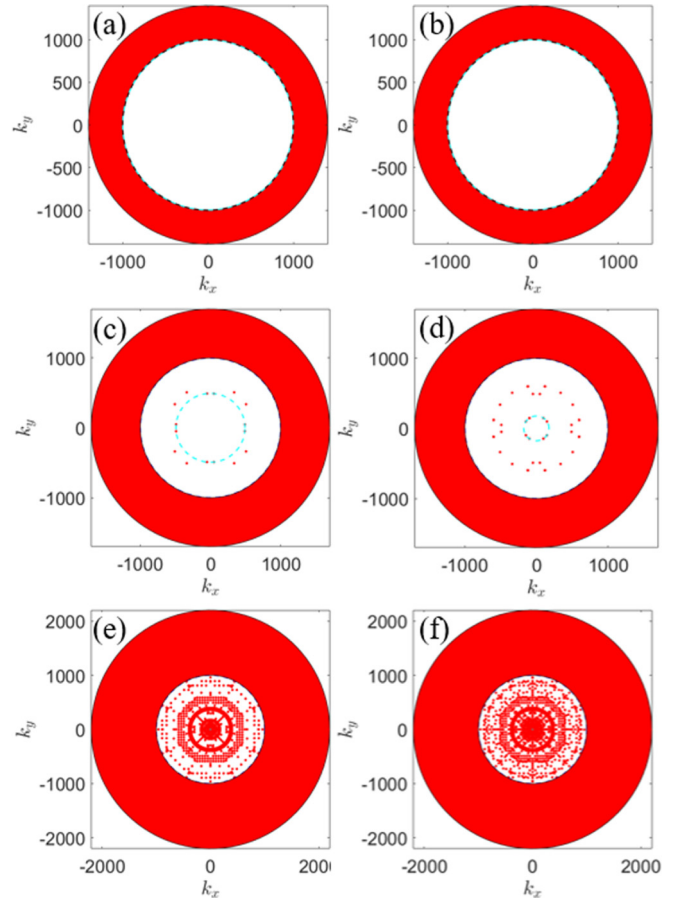
FIG. 3. The distribution of active wave modes (red dots) in the final state of inverse cascades with $r_I = 1000$, for (a) $R = 1400$, lower bound, (b) $R = 1400$, upper bound, (c) $R = 1700$, lower bound, (d) $R = 1700$, upper bound, (e) $R = 2200$, lower bound, and (f) $R = 2200$, upper bound. The initially excited region is indicated by the ring-shaped red area. The minimum wave number k_{min} of the active modes is indicated by a circle with cyan dashed line.
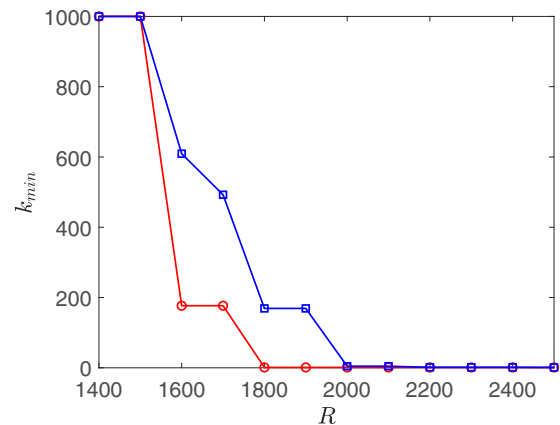
FIG. 4. The minimum wave number k_{min} as a function of the outer radius R in inverse cascades with $r_I = 1000$. Both upper (red line with squares) and lower (blue line with squares) bounds are shown.
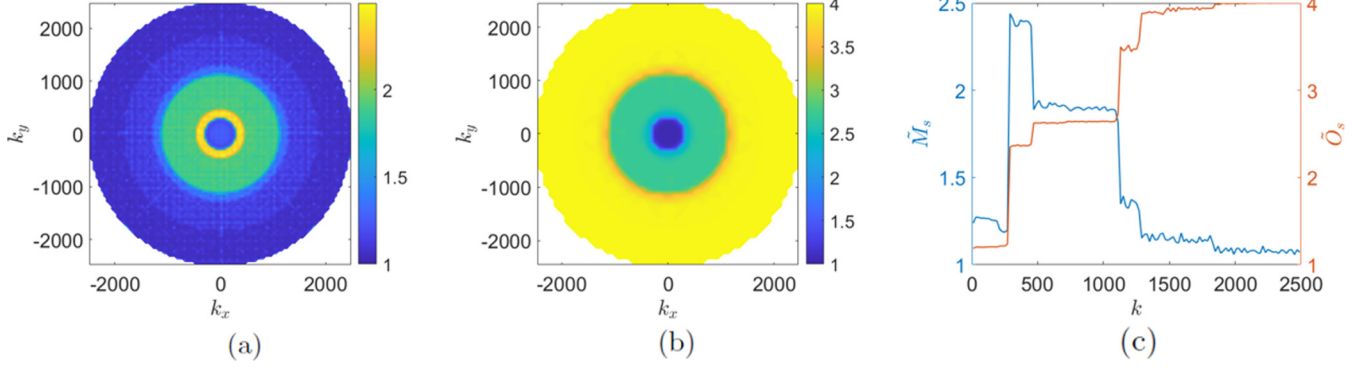
FIG. 5. The distribution of (a) M_s and (b) O_s in the (k_x, k_y) plane, and (c) $\tilde{M}_s$ and $\tilde{O}_s$ as functions of k with $R = 2500$. In (a) and (b), the values are averaged over the modes with nonzero $M_s(\boldsymbol{k})$ in a 50×50-grid area to avoid large discrete peaks in the original field.

be generated. As R increases beyond 1500, discrepancy between upper and lower bounds occurs, with stepwise transition behavior shown in the solutions. The frozen turbulence state transits to unlimited cascade for $R \in [1800, 2000]$, after which the upper and lower bounds become close to each other with $k_{\min}$ close to unity. We note that in numerical simulation of gravity-wave primitive equations with forcing in [28,32], a condensate forms at low wave numbers [14] indicating that quasiresonances are disabled toward large scales. Our study, with placement of initial modes in [28,32] and both direct or inverse cascades activated, further shows there is no exact resonance reaching unity in this corresponding case.

Finally, by examining the behavior of the upper and lower bounds in direct and inverse cascades, the role of angle resonances in the modal propagation can be inferred. It is clear in both cases that discrepancy between the two bounds occurs mainly when the initially active region is of appropriate size (i.e., not too small or too large). This is partly expected due to the finite wave number space, i.e., if the scale-resonance cascade can reach the boundary, angle resonances are not needed (so that the upper and lower bounds for large initial regions are guaranteed to be the same). However, it will be beneficial to conduct a more rigorous analysis to elucidate the full mechanism, as well as the sharp transition from frozen turbulence to unlimited cascade above $r_D \approx 60$ for direct cascade. Such an analysis is presented in Sec. IV.

IV. STRUCTURE OF RESONANT QUARTETS

In order to understand the state transition and role of angle resonances, it is necessary to discuss the structure of scale resonances in $\mathcal{Q}_s$. In particular, we aim to quantify the capability of a given mode in connecting smaller and larger scales through scale resonances, which also provides a hint on the role of angle resonances at this scale.

For this purpose, we define the scale-resonance multiplicity index $M_s(\boldsymbol{k})$ and order index $O_s(\boldsymbol{k})$:

$$M_s(\boldsymbol{k}) = |\{q : \boldsymbol{k} \in q\}|, \quad O_s(\boldsymbol{k}) = \overline{\{RK[\boldsymbol{k}; q] : \boldsymbol{k} \in q\}}, \quad (4)$$

where $q = \{\boldsymbol{k}_1, \boldsymbol{k}_2, \boldsymbol{k}_3, \boldsymbol{k}_4\}$ is a set taken from the quartets in $\mathcal{Q}_s$, $|\cdot|$ is the cardinality of the set, which in this context counts the number of q for which $\boldsymbol{k}$ is an element, $RK[\boldsymbol{k}; q]$ gives the ranking index of $\boldsymbol{k}$ in set q (1,2,3,4 for length from smallest to largest), and $\overline{\cdot}$ calculates the average of the num-

bers in the set, and in this context the average of ranking indices. With definition (4), $M_s(\boldsymbol{k})$ measures the number of scale resonances including mode $\boldsymbol{k}$ and $O_s(\boldsymbol{k})$ measures the average ranking of $\boldsymbol{k}$ (in terms of length) among all scale-resonant quartets. For a favorable situation of cascade crossing $\boldsymbol{k}$, it is desired that $M_s(\boldsymbol{k})$ is large and $O_s(\boldsymbol{k})$ is in the middle range (say, around 2.5).

Figures 5(a) and 5(b) show $M_s(\boldsymbol{k})$ and $O_s(\boldsymbol{k})$ in the domain $\mathcal{S}_{R=2500}$. We note that in the plot we consider only those modes for which $M_s(\boldsymbol{k})$ is nonzero, i.e., there exist some quartets in $\mathcal{Q}_s$ for which $\boldsymbol{k}$ is an element. In general, it can be seen that the function $M_s(\boldsymbol{k})$ peaks around the middle range of k, whereas $O_s(\boldsymbol{k})$ increases from 1 to 4 as k increases. The behaviors of $M_s(\boldsymbol{k})$ and $O_s(\boldsymbol{k})$ at large k can be partly explained by the finite wave number space $\mathcal{S}_R$, which eliminates many quartets (with modes beyond R), leading to $M_s(\boldsymbol{k}) \approx 0$ and $O_s(\boldsymbol{k}) \approx 4$. In order to more precisely quantify the two indexes at each (scalar) scale k, we further define the angle-averaged quantities:

$$\tilde{M}_s(k) = \overline{\{M_s(\boldsymbol{k}^*) : ||\boldsymbol{k}^*| - k| < \delta k/2, M_s(\boldsymbol{k}^*) \neq 0\}}, \quad (5)$$

$$\tilde{O}_s(k) = \overline{\{O_s(\boldsymbol{k}^*) : ||\boldsymbol{k}^*| - k| < \delta k/2, M_s(\boldsymbol{k}^*) \neq 0\}}, \quad (6)$$

with $\delta k = 20$ used in our calculation. We plot $\tilde{M}_s(k)$ and $\tilde{O}_s(k)$ in Fig. 5(c), which shows consistent behavior as Figs. 5(a) and 5(b) and helps elucidate the transition from frozen turbulence to unlimited cascade, as well as the role of angle resonances, as explained below.

In both direct and inverse cascades, if the initial active region is small (i.e., r_D and R are small for respectively the direct and inverse cascades), the cascade dies out close to the initial region. This is because the index $\tilde{O}_s(k)$ is close to either 1 and 4 for the direct and inverse cascade, and the index $\tilde{M}_s(k)$ is small for both cases, resulting in an unfavorable situation of generating new scales (by scale resonances). Under this situation, even if many angle resonances are included (in fact, for initial state the modes are already dense in the angular direction), the cascade will not be further excited. As the initial active region grows to appropriate size, $k_{\max}$ and $k_{\min}$ can reach the middle range in $\mathcal{S}_R$, where the scale of favorable cascade becomes active, i.e., scales with $\tilde{O}_s(k) \approx 2.5$ and large $\tilde{M}_s(k)$. We see from Fig. 5(c) that this favorable scale of energy transfer occurs as k grows above 250. Referring to Fig. 2, $k = 250$ corresponds to $r_D \approx 60$, which is exactly the

starting point of the sharp transition from frozen turbulence to unlimited cascade. For these cases, angle resonances become important as they excite more modes in the favorable scale k to sustain the cascade, leading to discrepancies in the upper and lower bounds of the solution. Finally, as the initial active region becomes large enough so that scale resonances themselves can sustain an cascade to the boundary of the domain (i.e., k_{max} reaching R and k_{min} reaching 1), angle resonances become unimportant for the extent of cascades. More precisely, they result in a difference in the density of active modes but do not affect k_{max} and k_{min}.

V. CONCLUSIONS AND DISCUSSION

In this paper, we have studied the cascade of surface gravity waves by exact resonances in a finite discrete wave number space. A kinematic model is developed based on the scale resonances and the upper and lower bounds of angle resonances, which significantly reduces the computational cost compared to the brute-force searching method used in previous studies. Both direct and inverse cascades are examined with different sizes of initially active regions. For direct cascade, we find that there exists a critical radius of the initial region within the range [60,110], above which the dynamics transits from frozen turbulence to unlimited cascade (with cascade extending to the boundary $R = 2500$). For inverse cascade, states of frozen turbulence and unlimited cascade are also observed but with a somewhat less sharp transition. We finally analyze the structure of resonant quartets, which helps to elucidate the sharp transition in [60,110] and the role of angle resonances in the extent of the cascades observed in the kinematic studies.

We remark that although the current study is for finite R, certain results obtained in the paper also apply for the case with $R \to \infty$. For example, the frozen turbulence state observed for $k < \sim 60$ applies because our value of R is sufficiently large to capture all possible four-wave resonances. So does the linear scaling $k_{max} \approx 5.5 r_D - 35.9$ obtained in the frozen turbulence regime. Physically if an experiment or simulation is conducted in domain size L with sufficient weak forcing or initial energy concentrated within wave number $120\pi / L$, the highest wave number that can be excited is described by the linear scaling.

APPENDIX: COMPUTATION OF SCALE RESONANCES

To find all the scale resonances satisfying the constraints in (3), we follow a generic method proposed in [31] to the system of surface gravity waves with the resonant conditions taking the form (2). The main idea of this method is to partition the spectral domain into disjoint classes of $\boldsymbol{k}$, which allows us to search for solutions in each class efficiently.

We first rewrite (2) in the following form:

$$
\begin{aligned}
m_1 + m_2 &= m_3 + m_4, \\
n_1 + n_2 &= n_3 + n_4, \\
\omega_1 + \omega_2 &= \omega_3 + \omega_4,
\end{aligned}
\tag{A1}
$$

where $\omega_i = |\boldsymbol{k}_i|^{1/2} = (m_i^2 + n_i^2)^{1/4}$ ($i = 1, 2, 3, 4$).

Now let's consider a set of algebraic numbers $\omega = t^{1/4}, t \in \mathbb{N}$. Any such number ω can be represented by

$$
\omega = \gamma q^{1/4}, \quad \gamma \in \mathbb{N},
\tag{A2}
$$

where q is a product

$$
q = p_1^{e_1} p_2^{e_2} \cdots p_n^{e_n},
\tag{A3}
$$

with $p_1, p_2, \ldots, p_n$ different primes and the powers $e_1, e_2, \ldots, e_n \in \mathbb{N}$ all smaller than 4. Then we define the set of numbers ω with the same q as the q-class denoted by Cl_q, where q is called the class index. For each $\omega = \gamma q^{1/4} \in Cl_q$, γ is called the weight of ω.

Based on these definitions, it can be shown that there are two types of solutions for (A1).

Case 1. All the numbers ω_i ($i = 1, 2, 3, 4$) belong to the same class Cl_q. In this case the third equation of (A1) can be written as

$$
\gamma_1 q^{1/4} + \gamma_2 q^{1/4} = \gamma_3 q^{1/4} + \gamma_4 q^{1/4}
\tag{A4}
$$

with $\gamma_i \in \mathbb{N}$ ($i = 1, 2, 3, 4$).

Case 2. The numbers ω_i belong to two different classes Cl_{q_1} and Cl_{q_2}. In this case the third equation of (A1) can be written as

$$
\gamma_1 q_1^{1/4} + \gamma_2 q_2^{1/4} = \gamma_1 q_1^{1/4} + \gamma_2 q_2^{1/4}
\tag{A5}
$$

with $\gamma_i \in \mathbb{N}$ ($i = 1, 2$).

It is evident that scale resonances, which generate modes with new lengths, are possible only in Case 1 since Case 2 consists of modes with pairwise equal lengths. Therefore, we concentrate on finding possible solutions in Case 1. The general idea is to take all solutions of $\gamma_1 + \gamma_2 = \gamma_3 + \gamma_4$ with $\gamma_i^4 q$ decomposable into the sum of two squares $\gamma_i^4 q = m_i^2 + n_i^2$ and then check the linear conditions [the first and second equations in (A1)]. The detailed description of this algorithm is as follows.

1. Procedures

a. Calculating class indexes

We first consider numbers $t_i = \omega_i^4 = \gamma_i^4 q$. To obtain a solution for (A1), t_i must have a representation as the sum of two squares of integers, i.e., $t_i = m_i^2 + n_i^2$. This requirement restricts the class index q in the following way: according to the Euler's theorem [46], an integer can be represented by the sum of two squares if and only if every factor with the form $p \equiv 4u + 3$ ($u \in \mathbb{N}$) contained in its prime factorization is in an even degree. As γ_i^4 already contains every prime factor in an even degree (the degree of any factor is an integer multiple of 4), this condition must be held for q. Note that by construction, all prime factors of q are in degrees smaller than 4. Therefore, the restriction for q becomes: if q is divisible by a prime $p \equiv 4u + 3$, it should be divisible by its square and not be divisible by its cube.

Based on the above requirements, the possible class indexes q for modes inside the spectral domain $\mathcal{S}_R$ ($q \leqslant R^2$) are calculated as follows. We create a list of integers $A_q = \{1, 2, \ldots, R^2\}$ and make two passes over it. In the first pass, we remove all the numbers divisible by the fourth power of any prime. In the second pass, we examine the numbers divisible by any prime satisfying $p \equiv 3 \mod 4$: if the number

is not divisible by p^2 or divisible by p^3, we remove it from A_q. Finally, A_q contains all the class indexes q that can be represented by the sum of two squares.

b. Solving the equation for weights

The next step is to solve the equations for the weights obtained from (A4),

$$\gamma_1 + \gamma_2 = \gamma_3 + \gamma_4, \tag{A6}$$

with $1 \leqslant \gamma_i \leqslant M(q)$, where $M(q) = \lfloor (R^2/q)^{1/4} \rfloor$ is the maximum possible weight γ for a given q with $\lfloor \cdot \rfloor$ being the round-down operator. Let $S_\gamma = \gamma_1 + \gamma_2 = \gamma_3 + \gamma_4$. Without loss of generality we can suppose

$$\gamma_1 \leqslant \gamma_3 \leqslant \gamma_4 \leqslant \gamma_2. \tag{A7}$$

There are four possible cases for the weights:

(1) $\gamma_1 < \gamma_3 < \gamma_4 < \gamma_2$,
(2) $\gamma_1 = \gamma_3 < \gamma_4 = \gamma_2$,
(3) $\gamma_1 < \gamma_3 = \gamma_4 < \gamma_2$,
(4) $\gamma_1 = \gamma_3 = \gamma_4 = \gamma_2$.

Since our aim is to find the scale resonances, we need to consider only cases (1) and (3) where the lengths of the four modes are not pairwise equal. Then the search of the solutions of (A6) is basically to find two partitions of S_γ ($\gamma_1 + \gamma_2$ and $\gamma_3 + \gamma_4$) satisfying cases (1) and (3), which can be computed straightforwardly by looping over all possible combinations of the partitions of S_γ under the condition that $1 \leqslant \gamma_i \leqslant M(q)$ ($i = 1, 2, 3, 4$).

Note that before this step, we can reduce the computational cost by discarding classes which consist of no solution in cases (1) and (3). Consider the classes with $M(q) = 1$; this means that all four weights $\gamma_i = 1$ ($i = 1, 2, 3, 4$). These classes correspond to the case (4), which have all four modes with the same length. Therefore, we can directly discard such classes without any computation of solving (A6). Similarly, we can also discard classes with $M(q) = 2$ since only cases (2) and (4) are possible in this condition. According to our calculation, there are 98.5% class with $M(q) = 1, 2$ among all the classes obtained in the domain $\mathcal{S}_{R=1000}$. Thus, discarding them significantly reduces the number of classes to be checked in the following steps.

c. Decomposition into sum of squares

The aim of this step is to find the decompositions of the number $\gamma_i^4 q$ with $\gamma_i = 1, 2, \ldots, M(q)$. The generalized form of this problem has been investigated in [47], which gives an efficient algorithm to search for all decompositions

Algorithm 2. Search for scale resonances.

Input: size of the domain R
Output: set of scale resonance quartets $\mathcal{Q}_s$
  1. Compute the list of class indexes $A_q = \{q : q \in \mathbb{N}^+, q \leqslant R^2; \exists x, y \in \mathbb{N}^+, q = x^2 + y^2\}$.
  2. Solve (A6) to obtain all possible γ_i ($i = 1, 2, 3, 4$) for each $q \in A_q$.
  3. Decompose $\gamma_i^4 q$ obtained in 1 and 2 into sum of two squares: $m_i^{*2} + n_i^{*2}$ ($m_i^*, n_i^* \in \mathbb{N}$).
  4. Check the linear conditions (A8) and put all qualified quartets $(\boldsymbol{k}_1, \boldsymbol{k}_2, \boldsymbol{k}_3, \boldsymbol{k}_4)$ with $\boldsymbol{k}_i = (\pm m_i^*, \pm n_i^*)$ into $\mathcal{Q}_s$.

of $b = x^2 + y^2$ ($x, y \in \mathbb{N}$). First, we search for all $a \in \mathbb{N}$ satisfying $a^2 \equiv (-1) \mod b$, $0 < a < b/2$. Then for each a we construct a finite sequence $\{r_j\}$ with $r_0 = b$, $r_1 = a$, $r_{j+2} = \beta_j r_{j+1} - r_j$, and $\beta_j = \lfloor r_j/r_{j+1} \rfloor$. It can be shown that $\exists N > 1$ ($N \in \mathbb{N}$) such that $r_0 > r_1 > \cdots > r_N = 1 > r_{N+1} = 0$. If we can find an integer k such that $r_{k-1}^2 > b > r_k^2$, then $b = r_k^2 + r_{k+1}^2$. Based on this method, we can obtain all the decomposition of $\gamma_i^4 q$ into sum of two squares of integers. Note that if $b = c^2(x^2 + y^2)$ with $c > 1$ ($c \in \mathbb{N}$), the above method cannot obtain such decomposition directly. Therefore, we need to check if $\gamma_i^4 q$ is divisible by an integer square before applying this method. In such conditions, we divide b by c^2 first and then compute the decomposition using the above method.

d. Checking linear conditions

Finally, we check the linear conditions [the first and second equations in (A1)] to find all solutions based on (m_i^*, n_i^*) ($m_i^* \geqslant 0$, $n_i^* \geqslant 0$, $i = 1, 2, 3, 4$) satisfying the third equation of (A1) obtained from the previous steps. This is done by taking all combinations of signs satisfying

$$\pm m_1^* \pm m_2^* = \pm m_3^* \pm m_4^*,$$
$$\pm n_1^* \pm n_2^* = \pm n_3^* \pm n_4^*. \tag{A8}$$

There are $2^8 = 256$ combinations in total for each set of (m_i^*, n_i^*). With the repeated solutions (e.g., some m_i^* or n_i^* being 0) and the symmetric solutions (e.g., all signs become opposite in the equations) taken into consideration, a correct, exhaustive, and efficient search can be constructed.

2. Summary

The full computation process is summarized in Algorithm 2.

---

[1] V. E. Zakharov, V. S. L'vov, and G. Falkovich, *Kolmogorov Spectra of Turbulence I: Wave Turbulence* (Springer Science & Business Media, Berlin, 2012).

[2] V. E. Zakharov, Stability of periodic waves of finite amplitude on the surface of a deep fluid, J. Appl. Mech. Tech. Phys. **9**, 190 (1972).

[3] V. E. Zakharov and N. Filonenko, Weak turbulence of capillary waves, J. Appl. Mech. Tech. Phys. **8**, 37 (1971).

[4] Y. V. Lvov, K. L. Polzin, and E. G. Tabak, Energy Spectra of the Ocean's Internal Wave Field: Theory and Observations, Phys. Rev. Lett. **92**, 128501 (2004).

[5] S. Galtier, S. Nazarenko, A. C. Newell, and A. Pouquet, A weak turbulence theory for incompressible magnetohydrodynamics, J. Plasma Phys. **63**, 447 (2000).

[6] S. Galtier and S. V. Nazarenko, Turbulence of Weak Gravitational Waves in the Early Universe, Phys. Rev. Lett. **119**, 221101 (2017).

[7] S. Y. Annenkov and V. I. Shrira, Role of non-resonant interactions in the evolution of nonlinear random water wave fields, J. Fluid Mech. **561**, 181 (2006).

[8] A. Hrabski and Y. Pan, On the properties of energy flux in wave turbulence, J. Fluid Mech. **936**, A47 (2022).

[9] A. Pushkarev, On the Kolmogorov and frozen turbulence in numerical simulation of capillary waves, Eur. J. Mech. B Fluids **18**, 345 (1999).

[10] A. I. Dyachenko, A. O. Korotkevich, and V. E. Zakharov, Decay of the monochromatic capillary wave, J. Exp. Theor. Phys. Lett. **77**, 477 (2003).

[11] A. O. Korotkevich, A. I. Dyachenko, and V. E. Zakharov, Numerical simulation of surface waves instability on a homogeneous grid, Physica D **321–322**, 51 (2016).

[12] Y. Deng and Z. Hani, On the derivation of the wave kinetic equation for NLS, in *Forum of Mathematics, Pi*, Vol. 9, e6 (Cambridge University Press, 2021).

[13] Y. Deng and Z. Hani, Full derivation of the wave kinetic equation, arXiv:2104.11204.

[14] A. Korotkevich, A. Pushkarev, D. Resio, and V. Zakharov, Numerical verification of the weak turbulent model for swell evolution, Eur. J. Mech. B Fluids **27**, 361 (2008).

[15] V. E. Zakharov, A. O. Korotkevich, A. N. Pushkarev, and A. I. Dyachenko, Mesoscopic wave turbulence, JETP Lett. **82**, 487 (2005).

[16] A. Hrabski and Y. Pan, Effect of discrete resonant manifold structure on discrete wave turbulence, Phys. Rev. E **102**, 041101(R) (2020).

[17] E. Faou, P. Germain, and Z. Hani, The weakly nonlinear large-box limit of the 2D cubic nonlinear Schrödinger equation, J. Amer. Math. Soc. **29**, 915 (2016).

[18] A. Pushkarev and V. Zakharov, Turbulence of capillary waves—Theory and numerical simulation, Physica D **135**, 98 (2000).

[19] Y. Pan and D. K. P. Yue, Direct Numerical Investigation of Turbulence of Capillary Waves, Phys. Rev. Lett. **113**, 094501 (2014).

[20] Y. Pan and D. K. Yue, Decaying capillary wave turbulence under broad-scale dissipation, J. Fluid Mech. **780**, R1 (2015).

[21] P. Denissenko, S. Lukaschuk, and S. Nazarenko, Gravity Wave Turbulence in a Laboratory Flume, Phys. Rev. Lett. **99**, 014501 (2007).

[22] R. Hassaini and N. Mordant, Confinement effects on gravity-capillary wave turbulence, Phys. Rev. Fluids **3**, 094805 (2018).

[23] Z. Zhang and Y. Pan, Numerical investigation of turbulence of surface gravity waves, J. Fluid Mech. **933**, A58 (2022).

[24] E. Falcon and N. Mordant, Experiments in surface gravity–capillary wave turbulence, Annu. Rev. Fluid Mech. **54**, 1 (2022).

[25] E. A. Kartashova, On properties of weakly nonlinear wave interactions in resonators, Physica D **54**, 125 (1991).

[26] E. A. Kartashova, Weakly Nonlinear Theory of Finite-Size Effects in Resonators, Phys. Rev. Lett. **72**, 2013 (1994).

[27] E. Kartashova, Wave resonances in systems with discrete spectra, *Nonlinear Waves and Weak Turbulence*, Amer. Math. Soc.

Transl. Ser. 2, Vol. 182 (Amer. Math. Soc., Providence, RI, 1998), pp. 95–129, doi: 10.1090/trans2/182/04.

[28] R. Carles and E. Faou, Energy cascades for NLS on the torus, Discrete Contin. Dyn. Syst. S **32**, 2063 (2012).

[29] J. Colliander, M. Keel, G. Staffilani, H. Takaoka, and T. Tao, Transfer of energy to high frequencies in the cubic defocusing nonlinear Schrödinger equation, Invent. Math. **181**, 39 (2010).

[30] Y. V. Lvov, S. Nazarenko, and B. Pokorni, Discreteness and its effect on water-wave turbulence, Physica D **218**, 24 (2006).

[31] E. Kartashova and A. Kartashov, Laminated wave turbulence: Generic algorithms I, Int. J. Mod. Phys. C **17**, 1579 (2006).

[32] M. Onorato, A. R. Osborne, M. Serio, D. Resio, A. Pushkarev, V. E. Zakharov, and C. Brandini, Freely Decaying Weak Turbulence for Sea Surface Gravity Waves, Phys. Rev. Lett. **89**, 144501 (2002).

[33] A. I. Dyachenko, A. O. Korotkevich, and V. E. Zakharov, Weak Turbulent Kolmogorov Spectrum for Surface Gravity Waves, Phys. Rev. Lett. **92**, 134501 (2004).

[34] N. Yokoyama, Statistics of gravity waves obtained by direct numerical simulation, J. Fluid Mech. **501**, 169 (1999).

[35] S. Nazarenko, M. Onorato, and D. Proment, Bose-Einstein condensation and Berezinskii-Kosterlitz-Thouless transition in the two-dimensional nonlinear Schrödinger model, Phys. Rev. A **90**, 013624 (2014).

[36] S. Galtier and S. V. Nazarenko, Direct Evidence of a Dual Cascade in Gravitational Wave Turbulence, Phys. Rev. Lett. **127**, 131101 (2021).

[37] M. Tsubota, K. Fujimoto, and S. Yui, Numerical studies of quantum turbulence, J. Low Temp. Phys. **188**, 119 (2017).

[38] G. Falkovich and N. Vladimirova, Cascades in nonlocal turbulence, Phys. Rev. E **91**, 041201(R) (2015).

[39] C. Connaughton, S. Nazarenko, and A. Pushkarev, Discreteness and quasiresonances in weak turbulence of capillary waves, Phys. Rev. E **63**, 046306 (2001).

[40] A. Hrabski, Y. Pan, G. Staffilani, and B. Wilson, Energy transfer for solutions to the nonlinear schrodinger equation on irrational tori, arXiv:2107.01459.

[41] E. Kartashova and A. Kartashov, Laminated wave turbulence: Generic algorithms II, Commun. Comput. Phys. **2**, 783 (2007).

[42] E. Kartashova and A. Kartashov, Laminated wave turbulence: Generic algorithms III, Physica A **380**, 66 (2007).

[43] E. Kartashova, Exact and Quasiresonances in Discrete Water Wave Turbulence, Phys. Rev. Lett. **98**, 214502 (2007).

[44] E. Kartashova, S. Nazarenko, and O. Rudenko, Resonant interactions of nonlinear water waves in a finite basin, Phys. Rev. E **78**, 016304 (2008).

[45] https://github.com/joezhang13/ExactResonance.

[46] L. Euler, Theoremata arithmetica nova methodo demonstrata, Novi Commentarii academiae scientiarum Petropolitanae **8**, 74 (1763), https://scholarlycommons.pacific.edu/euler-works/271.

[47] J. M. Basilla, On the solution of $x^2 + dy^2 = m$, Proc. Jpn. Acad. A **80**, 40 (2004).